Measurement of Absolute Unimolecular and Bimolecular Rate Constants for CH_3CHOO Generated by the *trans*-2-Butene Reaction with Ozone in the Gas Phase

Jill D. Fenske,† Alam S. Hasson, Andy W. Ho, and Suzanne E. Paulson*

Department of Atmospheric Sciences, University of California at Los Angeles, Los Angeles, California 90095-1565

Received: May 3, 2000; In Final Form: August 4, 2000

Ozone−alkene reactions form vibrationally excited Criegee intermediates (of the form R_1R_2COO), some of which, once thermalized, are thought to react with SO_2, H_2O, NO_x, aldehydes, and alcohols. Several studies using relative rate techniques or ab initio calculations have resulted in estimates for the rate coefficients of reactions of the thermalized biradicals. The ranges of measured and estimated rate coefficients span 2−6 orders of magnitude, depending on the reaction partner. Using an atmospheric pressure flow reactor, we have made the first absolute rate coefficient determinations for reactions of a thermalized Criegee intermediate, measuring rates for unimolecular decomposition and reaction with acetaldehyde. For the thermalized CH_3-CHOO formed in *trans*-2-butene ozonolysis, values for $k_{dec} = 76\ s^{-1}$ and $k_{ald} = 1.0 \times 10^{-12}\ cm^3\ molecule^{-1}\ s^{-1}$, accurate to within a factor of 3 and 6, respectively, were obtained.

Introduction

Ozone−alkene reactions have received much attention recently owing to evidence that these reactions are an important source of oxidizing radicals in the atmosphere. Alkenes make up the majority of non-methane hydrocarbon emissions globally,[1] and sources include automobile exhaust, industrial emissions, and plants. Because ozone is a relatively long-lived species in the troposphere, its gas-phase reaction with alkenes is an important oxidizing process during both day and night, and may be a dominant loss process for some alkenes.[2] Ozone−alkene reactions produce vibrationally excited intermediates (of the form R_1R_2COO), some of which, once thermalized, are thought to react with SO_2, H_2O, NO_x, aldehydes, and alcohols.

Both the nascent intermediates and the thermalized form have long been referred to as "Criegee intermediates." The structure of a Criegee intermediate has yet to be determined experimentally; however, several quantum chemical studies have made a convincing case that the nascent form is a carbonyl oxide (e.g., refs 3−6). The thermalized form may be either a dioxirane (R2) or a carbonyl oxide.[7] Recognizing this, we refer to the nascent product as a carbonyl oxide, and the thermalized form as a *thermalized Criegee intermediate* (TCI).

The TCI formation yields are about 40% for ethene[8−13] and from 3 to 40% for larger alkenes.[11,13−16] Reaction of these intermediates with SO_2 and H_2O may form H_2SO_4 and organic acids, respectively, and may thus be an important source for free acidity in the troposphere.[7,17] A series of elegant studies using relative rate techniques and ab initio calculations have resulted in estimates for the rate coefficients of reactions of TCI and are summarized in Table 1. The ranges of measured and estimated rate coefficients span 2−6 orders of magnitude, depending on the reaction partner. Using an atmospheric pressure flow reactor, we have made, as far as we are aware, the first absolute rate coefficient determination for a reaction of a thermalized Criegee intermediate. Our experiments provide determinations of the rate coefficients for unimolecular decomposition of the TCI formed in the O_3 reaction with *trans*-2-butene, as well as for its reaction with acetaldehyde.

Mechanism of Ozone−Alkene Reactions

The reaction of ozone with alkenes is believed to occur via cycloaddition of ozone across the double bond, forming a five-membered ring that decomposes, producing a carbonyl product and a carbonyl oxide (e.g., refs 18 and 19). Most of the initial carbonyl oxide is vibrationally excited and may either decompose or be collisionally thermalized by the surrounding gas. For *trans*-2-butene

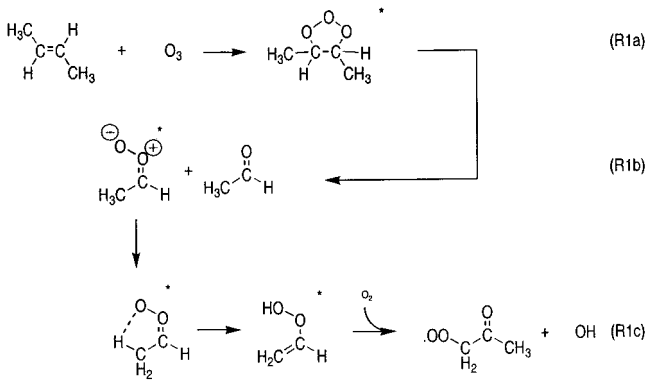

The carbonyl oxide may be formed in either a syn or anti configuration (R1b).

Recent theoretical calculations have shown that interconversion between these two carbonyl oxide isomers is restricted by an activation energy barrier of ∼30 kcal/mol.[5,20] Alternate pathways

* To whom correspondence should be addressed.
† Department of Chemical Engineering.

10.1021/jp0016636 CCC: $19.00
Published on Web 10/11/2000

TABLE 1: Summary of Rate Coefficients and Products for the Reactions of the Thermalized Criegee Intermediates (H_2COO except Where Noted)

reactant	ambient conn range (ppb)[m]	estimated k(298 K) (cm^3 $molecule^{-1}$ s^{-1})	rate in the boundary layer (s^{-1})[n]	expected products
H_2O	$3000-4 \times 10^7$	4×10^{-18} [a]	3×10^{34}	H_2O + organic acid[a]
	[1.6×10^6]	$2 \times 10^{-19}-1 \times 10^{-15}$ [b]	[0.16]	H_2O_2 + carbonyl[c]
		4×10^{-16} [c]		hydroxymethyl hydroperoxide[d] bis(hydroxymethyl)peroxide (in the presence of HCHO)[d]
SO_2	1−2000	7×10^{14} [a]	0.002−3	SO_3 + carbonyl
	[20]	7×10^{16} [e]	[0.03]	SO_2 + HCOOH[c]
		$3 \times 10^{-15}-1.7 \times 10^{-11}$ [b]		
		4×10^{-16} [c]		
CO	$120-5 \times 10^4$	1.3×10^{-16} [f]	$4 \times 10^{-4}-0.16$	CO_2 + carbonyl[g]
	[1000]	1.3×10^{-14} [c]	[0.003]	
NO_2	0.03−500	7×10^{-13} [a]	$5 \times 10^{-4}-9$	NO_3 + carbonyl[g]
	[50]	$1 \times 10^{-17}-7 \times 10^{-14}$ [b]	[0.9]	
		1×10^{-13} [c]		
NO	0.03−750	2×10^{-14} [i]	$1 \times 10^{-5}-0.4$	NO_2 + carbonyl
	[5]	7×10^{-12} [h]	[0.002]	
HCHO	0.05−50	1.2×10^{-14} [j]	$2 \times 10^{-5}-0.02$	$HOCH_2OCHO$
	[20]	2×10^{-17} [k]	[0.01]	(hydroxymethyl formate)[k]
		$2 \times 10^{-16}-8 \times 10^{-13}$ [b]		secondary ozonides
		2×10^{-14} [a]		
		2×10^{-12} [c]		
		CH_3CHOO: 4×10^{-16} [k]		
CH_3CHO		CH_3CHOO: 1×10^{-12} (this work)	negligible	secondary ozonide
decomposition		CH_2OO: 0.3 s^{-1} [l]		
		CH_3CHOO: 0.004−20 s^{-1} [b] 2.5 s^{-1} [k]	80 s^{-1} (this work)	
		$(CH_3)_2COO$: 250 s^{-1} [l]		

[a] Reference 30. [b] Reference 31. [c] Kerr and Calvert, as cited in ref 7. [d] References 28, 41, 52, and 53. [e] Based on an estimate that k_{SO_2} is larger than k_{H_2O} by a factor of 6×10^{-3},[7] and $k_{H_2O} = 4 \times 10^{-18}$. [f] Reference 8. [g] Proposed, not observed.[7,30] [h] Theoretical estimate.[30] [i] Theoretical estimate.[54] [j] Reference 8. [k] Reference 13. [l] Reference 39. [m] The ranges were assembled from Seinfeld[44] and Finlayson-Pitts and Pitts[19] for clean to very polluted air. The numbers in brackets are intended to be "representative" values to allow some comparison of the various reaction pathways. To calculate the value in brackets in column 4, we used the "moderate" concentration shown in column 2 and the reaction rate recommended by Atkinson and Lloyd.[30] The CO, SO_2, NO_2, and aldehyde concentrations are the lower limit of typical urban conditions.[44] A low NO concentration was chosen owing to the reaction between O_3 and NO in the atmosphere. Water value is 50% relative humidity at 298 K. [n] Based on the evaluation of Atkinson and Lloyd.[30]

with lower energy barriers, such as OH and dioxirane formation, may be more likely than interconversion. OH is a powerful oxidant in the atmosphere, and its formation from alkene ozonolysis has been widely studied.[21] Niki et al.[22] postulated that, for larger alkenes, OH formation occurs via the formation of a vibrationally excited unsaturated hydroperoxide from the carbonyl oxide, as in eq R1c. The vinyl hydroperoxide channel (R1c) is available only to the syn isomer and has an activation energy of about 15 kcal/mol for CH_3CHOO.[23] Formation of dioxirane (R2) requires 28 and 23 kcal/mol for syn and anti CH_3CHOO, respectively.[5]

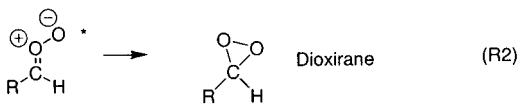

(R2)

Gutbrod et al.[23] performed CCSD(T) calculations that support this mechanism for OH formation from substituted carbonyl oxides.

Carbonyl oxides have not been observed directly in the gas phase; yields of thermalized Criegee intermediate have been inferred from measurement of product formation from secondary reactions with a variety of scavenger compounds (see below). Previously measured stabilized Criegee intermediate yields are in the range 0.13−0.24.[11,24−26] The rate coefficients investigated in this work are fairly sensitive to the TCI yield. Here, we have assumed the value of 0.185 reported by Hatakeyama et al.[7] and used the range of reported TCI yields (±0.06) to calculate the uncertainties for our rate coefficients.

Reactions of Thermalized Criegee Intermediates

Thermalized Criegee intermediates have been shown to react with several trace gas species, including H_2O, SO_2, CO, aldehydes, HO_2, alcohols, and carboxylic acids, and may undergo reaction with NO and NO_2.[7,8,13,27−30] The estimated and measured rate coefficients are summarized in Table 1. Since this study focuses on reaction with aldehydes and decomposition, these are briefly reviewed here.

Reaction with Aldehydes

The reactions of Criegee intermediates with aldehydes, while unimportant in the atmosphere, are central to experimental studies because aldehydes are cogenerated with Criegee intermediates in ozone−alkene reactions and have been the subject of several studies.[13,27,31−33] The estimated rate coefficients span the range $2 \times 10^{-12}-2 \times 10^{-17}$ cm^3 $molecule^{-1}$ s^{-1} (Table 1). The proposed product from the reaction of the simplest Criegee intermediate with formaldehyde is formic acid, which can react with a second Criegee intermediate to form hydroperoxymethyl formate:[34,35]

$$HCHO + CH_2OO \rightarrow HCHO + HCO_2H \qquad (R3)$$

For larger, substituted Criegee intermediates, secondary

$$CH_2OO + HCO_2H \rightarrow HOOCH_2OCHO \qquad (R4)$$

ozonides (SOZ) have been observed (e.g., refs 27, 32, 33, and 36):

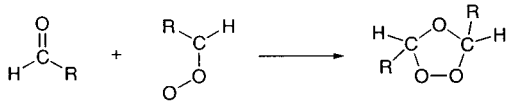

(R5)

Secondary ozonide formation from *trans*-2-butene ozonolysis has been verified by gas chromatography/mass spectroscopy (GC/MS)[32,33] and Fourier transform infrared (FTIR) spectroscopy.[27] The strongest IR absorption band for *trans*-2-butene secondary ozonide occurs at approximately 1130 cm^{-1}.[27,33] Fajgar et al.[33] synthesized secondary ozonides at low temperature in the liquid phase, used GC/MS and FTIR spectroscopy to confirm their structure, and found a strong IR band at 1128 cm^{-1}. They observed the same bands in the gas-phase ozonolysis of *trans*-2-butene, confirming formation of the secondary ozonide in the gas phase. Neeb et al.[27] also observed a secondary ozonide IR band at 1130 cm^{-1} from 2-butene ozonolysis. This is the band used in this study to monitor secondary ozonide formation; a representative secondary ozonide IR spectrum is shown in Figure 1.

Foreign aldehydes, when added in sufficient concentrations, may be used to trap the TCI. For example, Neeb et al.[27] added excess acetaldehyde to the ozonolysis of ethene and quantified propene ozonide by comparison with reference spectra of synthesized ozonides. The yield of secondary ozonide under these conditions was 40% (equal to the yield of TCI), and none of the products from the reaction of the TCI with formaldehyde (formic acid and hydroperoxy methyl formate) was observed. They found similar results upon adding acetone to ethene ozonolysis, indicating that it is possible to trap the TCI with a species that is not cogenerated, and thus that the nascent carbonyl oxide and carbonyl products separate completely. This is in contrast to the suggestion that the carbonyl oxide and aldehyde remain complexed.[37,38]

Horie and Moortgat[13] probed consumption of formaldehyde and formation of reaction products in a CSTR-type reactor to derive rate coefficients of formaldehyde with CH_2OO and CH_3CHOO. Using a chemical model, they calculated rate coefficients of 2×10^{-17} and 4×10^{-16} cm^3 $molecule^{-1}$ s^{-1}, for reaction of formaldehyde with CH_2OO and CH_3CHOO, respectively. No estimates have been made for the rate coefficient of the reaction of CH_3CHOO with CH_3CHO.

Decomposition of Thermalized Criegee Intermediates

While the unimolecular decomposition of vibrationally excited Criegee intermediates is well documented, the corresponding decomposition of TCI is generally not considered to be significant. However, the presence of a decomposition channel for TCI has been suggested by a few recent studies. Becker et al.[28] performed studies of the reaction of H_2O with CH_2OO and $(CH_3)_2COO$ using a relative rate technique based on the value for k_{SO_2} estimated by Atkinson and Lloyd (7×10^{-14} cm^3 $molecule^{-1}$ s^{-1}).[30] They note in this study that their product yields are lower than expected, and this may be due to an unaccounted-for decomposition channel for the Criegee intermediates studied. Olzmann et al.[39] performed a theoretical study of ethene and 2,3-dimethyl-2-butene ozonolysis. Using master equation analysis, they estimated the upper limit for the lifetimes of the thermalized Criegee intermediates to be 3 s for CH_2OO and 0.004 s for $(CH_3)_2COO$ with respect to unimolecular decomposition. Olzmann et al.[39] point out that the lifetimes of the unthermalized Criegee intermediates may be much shorter, as the calculated values for the lifetimes of CI obeying steady-state energy distributions were 10^{-9} and 10^{-7} s for CH_2OO and $(CH_3)_2COO$, respectively. Herron et al. [31] estimated that, for thermalized CH_3CHOO, 4×10^{-3} $s^{-1} < k_{dec} < 20$ s^{-1}, on the basis of relative rate arguments using an estimate of $k_{SO2-CH3CHOO}$. The study by Horie and Moortgat[13] (discussed above) resulted in a suggested decomposition rate coefficient for CH_3CHOO of 2.5 s^{-1}.

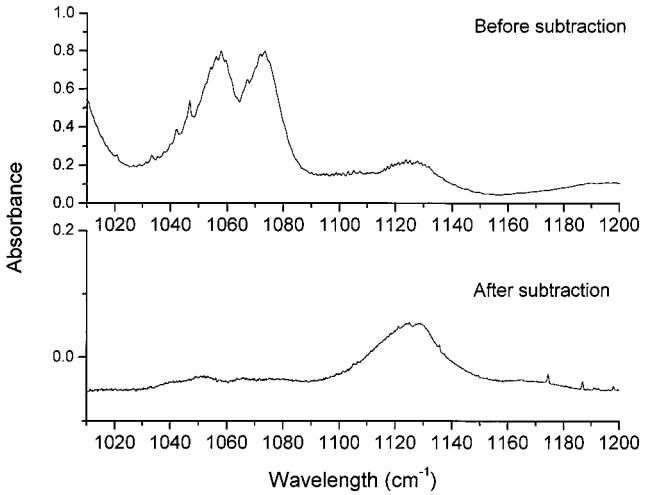

Figure 1. Secondary ozonide IR peak from *trans*-2-butene ozonolysis. This spectrum is from the 9.8.99 experiment with the injector at 0 cm. The upper spectrum is before any subtractions. The lower spectrum has *trans*-2-butene, acetaldehyde, and methanol subtracted out, and shows the SOZ peak used to obtain the data presented here.

Experimental Description

All experiments to measure CH_3CHOO kinetics were performed in a flow tube, shown schematically in Figure 2. The flow tube is constructed from a 2 cm i.d. × 2 m glass tube equipped with stainless steel end plates, which provide connection ports for the transfer tubing. Separate inlet ports introduce the alkene and ozone, and a small "turbulizer" (a fan-shaped piece of Teflon) provides thorough mixing as soon as the gas flows enter the tube. Concentrations of reactants and products were determined using Fourier transform infrared spectroscopy (FTIR) in a 50 L multireflection long-path cell (with a base path length of 1.5 m and variable path length from 36 to 140 m) (Infrared Analysis). Ozone was produced with a mercury lamp ozone generator (JeLight PS-3000-30) using a synthetic air mixture. The acetaldehyde bulb was prepared on a vacuum line and contained a high concentration (>10 000 ppm) of acetaldehyde. The acetaldehyde (Aldrich 99.5+%) was evaporated into the vacuum line to a pressure of approximately 200 Torr, and the bulb was pressurized to approximately 1100 Torr with nitrogen. *trans*-2-Butene (Aldrich 99+%) was used as a pure gas. All compounds were used as received. The carrier gas was a synthetic mix of nitrogen and oxygen (80% and 20%, respectively) (Lehner-Martin, liquid grade). Flow controllers (Unit Instruments model 8100 and model 3020A) provided constant flows of the aldehyde/N_2 mix and synthetic air; the *trans*-2-butene was controlled with a flow meter. The flow controllers had a stated uncertainty of ±1%. Calibration curves for the IR spectral features of acetaldehyde and *trans*-2-butene were determined from known concentrations of these compounds in the FTIR cell introduced using a calibrated volume

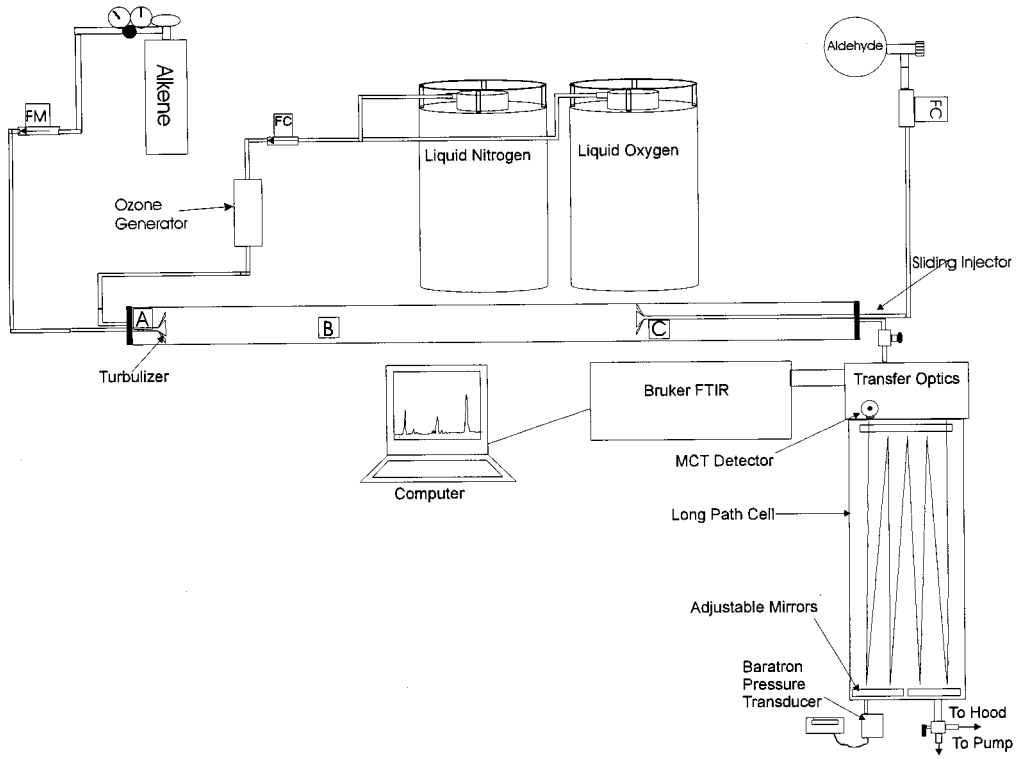

Figure 2. Flow tube apparatus. The ozone and alkene are added at the head of the flow tube (A). In the reaction zone (B), the ozone reacts with the alkene to generate CH_3CHOO, acetaldehyde, and other products. Some CH_3CHOO reacts with acetaldehyde to generate secondary ozonide (SOZ). Excess acetaldehyde is added through the sliding injector (C) to trap all of the thermalized Criegee intermediates present at the injector plus all thermalized Criegee intermediates that are generated postinjector as SOZ. SOZ is detected in the FTIR cell. FM = flow meter, FC = flow controller.

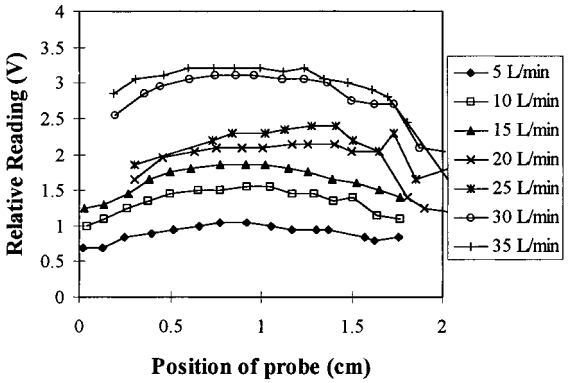

Figure 3. Velocity profiles for flows of 5−30 L/min, corresponding to Reynolds numbers of 350−2100. Measurements made with a hot-wire anemometer are plotted as voltage (relative to voltage at zero flow) versus position of probe (measured from one wall). These measurements were made at the end of the flow tube ($x = 1.8$ m), where the flow is expected to have the most deviation from a flat profile

and gas-handling line. The bands used to quantify *trans*-2-butene and acetaldehyde were at 2575−2625 and 2700 cm^{-1}, respectively.

The flow tube was operated in the developing flow regime, and thus a flat velocity profile is anticipated throughout the length of the tube. Turbulizers at the beginning of the tube and at the tip of the injector also ensure thorough mixing and facilitate a plug-flow profile. A reasonably flat velocity profile was observed using a hot-wire anemometer (TSI 1053B) to measure the flow velocity as a function of radial position across the tube (Figure 3). The radial velocity measurements were performed using a flow tube with the same dimensions as the one used for the experiments described below, but with openings every 25 cm for insertion of the anemometer probe. All openings not being used during a particular measurement were sealed, and the anemometer probe was mounted through a rubber stopcock equipped with O-rings to prevent leaks around the probe body.

Experimental Design

To verify the performance of the flow tube for kinetics studies, we measured the rate coefficient for the reaction of ozone with *trans*-2-butene under pseudo-first-order conditions. Ozone and *trans*-2-butene were mixed at the head of the flow tube, and the reaction was stopped by adding excess NO through the sliding injector at points along the tube. The concentration of acetaldehyde was monitored with FTIR spectroscopy as a function of injector position (and hence reaction time). Acetaldehyde formation as a function of reaction time was also calculated using the model shown in Table 2 with the rate coefficient of the *trans*-2-butene reaction with ozone as the only adjustable parameter. This rate coefficient was adjusted to minimize the differences between the calculated and measured acetaldehyde concentrations.

Experiments to investigate TCI (CH_3CHOO) kinetics were performed by adding ozone and *trans*-2-butene at the head of the flow tube. The TCI was trapped at various points along the tube by adding excess acetaldehyde through a sliding injector (Figure 2). Detection of reactants and products was accomplished with long-path FTIR spectroscopy. The secondary ozonide detected in the FTIR cell was the sum of that formed in the reaction zone by reacting with cogenerated aldehyde, plus any TCI generated in the reaction zone that had not already decomposed, plus all TCI generated after the injector. The residence time in the flow tube ranged from 1.3 to 3.1 s, corresponding to Reynolds numbers between 850 and 2120. The total flow was adjusted to between two and four lifetimes of

TABLE 2: Reaction Scheme Used for Calculations of Species Concentrations

no.	rate coefficient[a]	reactants	products
1	2.1E−16[b]	$CH_3CH{=}CHCH_3 + O_3$	→ 1.14CH_3CHO + 0.65OH + 0.65$OOCH_2CHO$ + 0.07CO + 0.07CH_3OH + 0.11CO_2 + 0.185 CH_3CHOO
2	1.1E−12	$CH_3CHOO + CH_3CHO$	→ SOZ
3	76 s^{-1}	CH_3CHOO	→ DECOMP
4	6.4E−11	$CH_3CH{=}CHCH_3 + OH$	→ $RCH(O)CH_2OO$
5	1.4E−11	$CH_3CHO + OH$	→ $CH_3C(O)OO + H_2O$
6	2.1E−12	$OOCH_2CHO + OOCH_2CHO$	→ 2.0HCHO + HO_2 + 0.5ROH + 0.5 RCH(O)
7	1.5E−11	$OOCH_2CHO + HO_2$	→ ROOH + O_2
8	3.1E−13	$RCH(O)CH_2OO + RCH(O)CH_2OO$	→ 4CH_3CHO + 2HO_2
9	2.2E−13	$RCH(O)CH_2OO + RCH(O)CH_2OO$	→ ROH + $CH_3C(O)CH_3$
10	1.6E−11	$RCH(O) + OH$	→ $CO_2 + H_2O + CH_3OO$
11	3.E−12	$CH_3C(O)OO + HO_2$	→ $CH_3C(O)OOH + O_2$
12	1.66E−11	$CH_3C(O)OO + CH_3C(O)OO$	→ 2CH_3OO + 2CO_2
13	3.7E−13	$CH_3OO + CH_3OO$	→ 0.72HO_2 + 1.29HCHO + 0.57CH_3OH + 0.07ROOH
14	5.8E−12	$CH_3OO + HO_2$	→ $CH_3OOH + O_2$
15	7E−13	$CH_3OO + OOCH_2CH$	→ 0.86HO_2 + 1.64HCHO + 0.53ROH + 0.04ROOH + 0.25RCH(O) + 0.34ROH + 0.34RCH(O) + 0.5HO_2
16	1E−12	$CH_3OO + RCH(O)CH_2OO$	→ 1.16$CH_3C(O)CH_3$ + 0.94HO_2 + 0.5ROH+ 0.21RCH(O) + 0.64HCHO + 0.04ROOH
17	1.7E−12	$OOCH_2CHO + RCH(O)CH_2OO$	→ 1.16CH_3CHO + 1.08HO_2 + 0.46ROH + 0.46RCH(O)OO
18	8.3E−6 s^{-1}	CH_3OOH	→ OH + HO_2 + HCHO
19	1.E−11	$OH + CH_3OOH$	→ CH_3OO + HCHO + OH + 2H_2O
20	1.E−11	OH + ROOH	→ 0.65RO_2 + 0.65CH_3CHO + 0.35OH
21	8.3E−6 s^{-1}	ROOH	→ OH + HO_2 + RCH(O)
22	1.6E−11	HCHO + OH	→ HO_2 + CO + H_2O
23	7.7E−15	$HCHO + HO_2$	→ $H_2C(O)OOH$
24	2.E12 s^{-1}	$H_2C(O)OOH$	→ HO_2 + HCHO
25	8.3E−6 s^{-1}	$CH_3C(O)OOH$	→ OH + HO_2 + HCHO
26	1.E−11	$OH + CH_3C(O)OOH$	→ $CH_3C(O)OO$ + HCHO + OH + 2H_2O
27	3.04E−11	RCH(O) + OH	→ RO_2
28	6.7E−12	$OH + CH_3OH$	→ HO_2 + HCHO + H_2O
29	3.8E−12	ROH + OH	→ 0.04HO_2 + 0.04HCHO + 0.21HCHO + 0.21HO_2 + 0.04$CH_3CH(O)OO$ + 0.47$RCH(O)CH_2OO$ + 0.24RC(O)(CH3)OO
30	3.E−13	$RO_2 + RO_2$	→ 2RCH(O) + 1.2HO_2
31	3.E−12	$RO_2 + HO_2$	→ ROOH
32	1.E−11	ROOH + OH	→ RCH(O) + OH + RO_2
33	2.4E−13	OH + CO	→ HO_2 + CO_2
34	1.60E−12	$OH + O_3$	→ $HO_2 + O_2$
35	1.0E−14	$HO_2 + O_3$	→ OH + 2O_2
36	2.3E−13	$HO_2 + HO_2$	→ $HOOH + O_2$
37	1.7E−33	$HO_2 + HO_2$ + M	→ $HOOH + O_2$
38	3.1E−34	$HO_2 + HO_2 + H_2O$	→ $HOOH + O_2 + H_2O$
39	6.6E−35	$HO_2 + HO_2 + H_2O$	→ $HOOH + O_2 + H_2O$
40	3.30E−12	HOOH + OH	→ $HO_2 + H_2O$
41	1.1E−10	$OH + HO_2$	→ $H_2O + O_2$

[a] All rate coefficients in cm^3 $molecule^{-1}$ s^{-1}, except for reactions 3, 18, 21, 24, and 25, which are in s^{-1}, and reactions 37−39, which are in cm^6 $molecule^{-2}$ s^{-1}. [b] Read as 2.1×10^{-16}.

ozone with respect to *trans*-2-butene reaction within the flow tube (>90% O_3 reacted): two lifetimes of ozone for low initial *trans*-2-butene concentrations and four lifetimes for high initial *trans*-2-butene concentrations.

The starting point for the CH_3CHOO kinetics experiments was to observe the quantity of secondary ozonide formed with no added excess acetaldehyde. Next, excess acetaldehyde was added at the head of the flow tube through the sliding injector, to trap all of the TCI as it formed. The acetaldehyde concentration was increased until the observed secondary ozonide signal reached a maximum, ensuring that the excess aldehyde was trapping all of the TCI generated postinjector. After that, the disappearance of TCI along the length of the tube was determined by varying the position of the sliding injector. By varying the concentrations of *trans*-2-butene and ozone (thus varying the TCI generation rate and concentration and the cogenerated aldehyde concentration) in the flow tube, a quantitative understanding of the processes consuming TCI may be obtained. The rate constants for disappearance of the TCI were determined both by using a chemical model to solve the differential equations describing the complete chemistry, including the reactions of the products, wall losses, and so forth, and with a simplified set of reactions that may be solved analytically (below).

Finally, a set of experiments using the FTIR cell as a batch reactor allowed an independent investigation of the dependence of secondary ozonide formation on acetaldehyde concentration. These experiments may also be compared with measurements

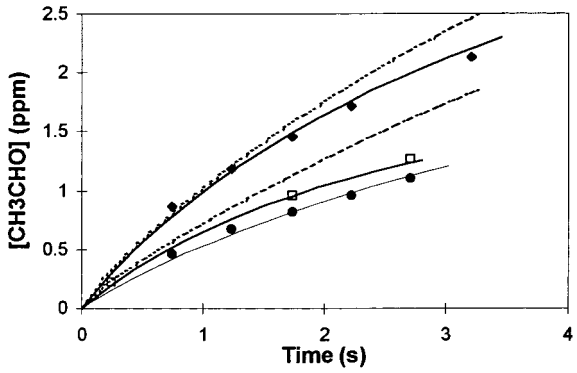

Figure 4. Data for measurement of the ozone−*trans*-2-butene rate coefficient: solid diamonds, experiment 4.15.99; open squares, experiment 4.9.99; solid circles, experiment 4.13.99. The solid line represents the best model fit, and dashed lines represent ±20% of the calculated result for 4.15.99.

TABLE 3: Summary of Measurements of the Rate Coefficient for Ozone Reaction with *trans*-2-Butene

experiment no.	$[O_3]_0$ (ppm)	$[T2B]_0$ (ppm)	k_{O3-t2B} (cm^3 $molecule^{-1}$ s^{-1})
4.9.99	46.2	2.00	1.6×10^{16}
4.13.99	20.7	2.69	2.0×10^{16}
4.15.99	28.7	3.89	2.0×10^{16}
average			$(1.9 \pm 0.3) \times 10^{16}$

made in batch reactors from the literature (see below). *trans*-2-Butene and acetaldehyde were added to the FTIR cell through a gas-handling manifold and brought to within 100 Torr of atmospheric pressure with nitrogen. Aliquots of ozone were then added by flowing pure oxygen through the ozone generator. The disappearance of *trans*-2-butene and the formation of secondary ozonide were quantified by FTIR spectroscopy. The initial concentration of added acetaldehyde was varied between 0 and 330 ppm with the initial concentration of *trans*-2-butene held at 30 ppm.

Results

***trans*-2-Butene + Ozone Kinetics.** Figure 4 shows all data from the *trans*-2-butene−O_3 kinetics measurements along with the best fits calculated with the chemical model. Table 3 summarizes the initial conditions and results. Because it was not possible to monitor either *trans*-2-butene or O_3 owing to interfering IR bands and direct reaction with NO, respectively, this reaction was followed by measuring the concentration of its major product, acetaldehyde. The *trans*-2-butene ozonolysis rate coefficient was derived by calculating acetaldehyde production from O_3 and OH reactions with trans-2-butene and acetaldehyde loss due to OH reaction using a numerical model (R1, R4, R5, R8, and R9, Table 2). The average value obtained for the O_3–*trans*-2-butene rate coefficient was $(1.9 \pm 0.3) \times 10^{-16}$ cm^3 $molecule^{-1}$ s^{-1}, in excellent agreement with the value recommended by Atkinson, $(1.9 \pm 0.7) \times 10^{-16}$ cm^3 $molecule^{-1}$ s^{-1}, [21] verifying good performance of the flow tube.

Batch Reactor Relative-Rate Experiments. The SOZ yield per molecule of O_3 reacted is plotted versus acetaldehyde concentration for several batch-reactor FTIR cell experiments in Figure 5. The amount of O_3 reacted was determined by multiplying the total amount of *trans*-2-butene reacted by the fraction of *trans*-2-butene expected to react with O_3 (as opposed to with OH radicals). From these data, it is clear that the yield of secondary ozonide is dependent upon the concentration of

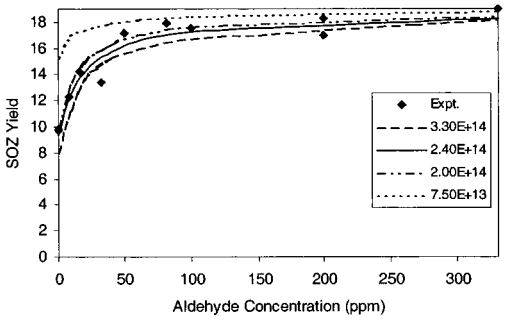

Figure 5. Yield of secondary ozonide (SOZ) from the ozone−*trans*-2-butene reaction as a function of added CH_3CHO concentration for batch reactor experiments.

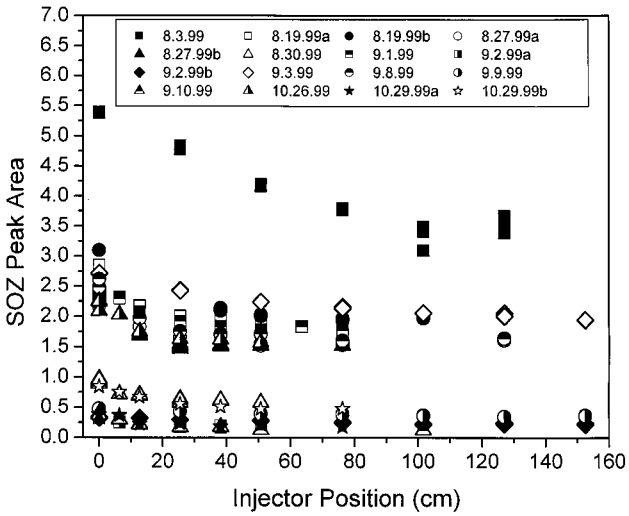

Figure 6. Kinetics data before subtraction of postinjector SOZ formation. The symbols in Figures 7−11 represent the same experiments throughout as noted in the legend.

aldehyde added to the reaction, reaching a limiting value at high aldehyde concentrations. The limiting value of the secondary ozonide yield was assumed to correspond to the TCI yield from *trans*-2-butene + O_3 (0.185).[11] SOZ generated at excess aldehyde concentrations was used to make a calibration curve of the SOZ peak area versus concentration of SOZ.

The observation that the production of SOZ increases as acetaldehyde is added indicates that the TCI have a limited lifetime. Figure 5 shows that roughly twice as much SOZ is formed with excess acetaldehyde than with no added acetaldehyde. Thus, the time scale of the second loss process for CH_3CHOO must be approximately equal to the time scale of reaction with acetaldehyde in the experiment with no added acetaldehyde, $k \sim k_{ald}[CH_3CHO]$, where k is the rate coefficient for the secondary loss process and k_{ald} is the acetaldehyde rate coefficient, and the ratio of k/k_{ald} is about 1×10^{14} molecules cm^3.

Flow Tube Measurements of CH_3CHOO Reactions. Raw data for the kinetics measurements of the reactions of CH_3CHOO are shown in Figure 6 and consist of the secondary ozonide concentration as a function of acetaldehyde injector position. The initial conditions and results are summarized in Table 4. The SOZ peak area is a maximum when the injector is at 0 cm, where the added excess aldehyde traps all of the TCI. The area of the SOZ peak decreases as the injector is moved away from the head of the tube, leveling off at a point corresponding with >90% of the ozone reacted. The measurement of the rate coefficient of CH_3CHOO with acetaldehyde would ideally be made with spatially distinct regions for

TABLE 4: Summary of Flow Tube Experiments To Measure the Rate Coefficients for the Disappearance of Thermalized Criegee Intermediates

experiment no.	$[T2B]_0$ (ppm)	$[O_3]_0$ (ppm)	k_{dec} (s^{-1})	k_{ald} (cm^3 $molecule^{-1}$ s^{-1})	k_{dec}/k_{ald}	k_{dec}/k_{ald} analytical
8.3.99	116	7.8	70	6×10^{-13}	1.2×10^{14}	1.2×10^{14}
8.19.99a	1190	10.1	70	8×10^{-13}	8.8×10^{13}	6.9×10^{13}
8.19.99b	678	10.1	75	7×10^{-13}	1.1×10^{14}	7.9×10^{13}
8.27.99a	738	7.5	65	9×10^{-13}	7.2×10^{13}	4.4×10^{13}
8.27.99b	1240	7.5	60	9×10^{-13}	6.7×10^{13}	5.8×10^{13}
8.30.99	1190	3.7	40	1×10^{-12}	4.0×10^{13}	4.3×10^{13}
9.1.99	1200	9.8	55	9×10^{-13}	6.1×10^{13}	1.5×10^{14}
9.2.99a	1070	1.7	110	1.9×10^{-12}	5.8×10^{13}	4.3×10^{13}
9.2.99b	214	1.7	30	1.4×10^{-12}	2.1×10^{13}	3.6×10^{13}
9.3.99	140	10.9	100	6×10^{-13}	1.7×10^{14}	1.6×10^{14}
9.8.99	1050	10.5	120	1×10^{-12}	1.2×10^{14}	7.4×10^{13}
9.9.99	99.4	2.10	70	1.6×10^{-12}	4.4×10^{13}	1.6×10^{13}
9.10.99	1060	1.60	120	1.1×10^{-12}	1.1×10^{14}	5.0×10^{13}
average			76 ± 29	$(1.0 \pm 0.4) \times 10^{-12}$	$(8.3 \pm 4.1) \times 10^{13}$	$(7.2 \pm 4.4) \times 10^{13}$
10.26.99[a]	1162	8.9	80	1.1×10^{-12}		
10.29.99a[a]	1146	2.0	80	1.8×10^{-12}		
10.29.99b[a]	1150	4.0	70	1.1×10^{-12}		
average			77 ± 6	$(1.3 \pm 0.4) \times 10^{-12}$		
overall avg.			76 ± 25	$(1.1 \pm 0.4) \times 10^{-12}$	$(7.0 \pm 4) \times 10^{13}$	

[a] These experiments carried out in a flow tube coated with halocarbon wax.

generation of the TCI (defined by complete consumption of O_3) and for introduction of the reaction partner through a sliding injector. However, the TCI did not survive in measurable quantities to be trapped after the generation zone. Further, a reaction partner other than the cogenerated aldehyde would have been ideal to trap the TCI. Several reagents were tested for their potential to trap TCI, including water,[28,40,,41] aldehydes,[27,32,33] and organic acids.[34,35,42] Secondary ozonides form under all conditions from the TCI reaction with cogenerated acetaldehyde. The secondary ozonide bands are broad with maxima centered close to one another: for example, 1130 and 1120 cm^{-1} for the $CH_3CHOO + CH_3CHO$ and $CH_3CHOO + HCHO$ secondary ozonides, respectively.[27] Thus, making a quantitative measurement of a mixture of secondary ozonides is difficult, precluding the use of an aldehyde other than acetaldehyde as a trapping reagent. Because water reacts approximately 10 000 times more slowly than the cogenerated acetaldehyde with TCI (see Table 1), very high concentrations (>10 000 ppm) are required to trap all of the TCI present at any point along the flow tube. We were unable to maintain such concentrations at the total flow rates (approximately 30 L min^{-1}) necessary to resolve the kinetics of CH_3CHOO. Using formic acid to trap the TCI was not possible because quantification of the CH_3CHOO-formic acid product, $HOO-CH(CH_3)-O-CHO$,[27] was confounded by subtraction residuals from the large formic acid peaks.

The uncertainties in the spectral subtractions to obtain the SOZ areas (Figure 1) are higher for low initial ozone concentrations (corresponding to low SOZ concentrations) than those for high initial ozone concentrations. For initial ozone concentrations of approximately 10 ppm, the uncertainty in the subtractions is about ±5%. The uncertainty increases to ±10% as the ozone concentration is decreased to 4 ppm. For initial ozone concentrations of 2 ppm and less, the uncertainty in the subtractions may be as large as a factor of 2.

For many of the analyses described below, yield calculations are made on a per molecule of *ozone* reacted basis, and after the SOZ formed postinjector (region C, Figure 2) has been subtracted from the total SOZ signal. The acetaldehyde added by the injector converts to SOZ all TCI that results from postinjector O_3-alkene reaction. To remove this offset from the SOZ data, we calculate the extent of O_3-alkene reaction at the point of the injector, multiply the remaining O_3 by the TCI yield of 0.18, and subtract this from the SOZ signal. This is a slight overestimation of the amount of SOZ formed at time *t* because it neglects the steady-state concentration of TCI at time *t*, but this is small ($<10^{10}$ molecules cm^{-3}) relative to the SOZ concentration ($10^{12}-10^{13}$ molecules cm^{-3}). It would obviously be preferable to measure the O_3 concentration at the injector, but this is impractical.

An OH radical scavenger was not used in these experiments. The high quantities of scavenger (or its reaction products) required to suppress the OH concentration would potentially result in large IR bands in the region of the SOZ peak, causing uncertainties in the SOZ quantification. In addition, potential effects of the chemistry of the scavenger and associated reaction products could introduce additional bimolecular reaction pathways for the TCI. OH is suppressed in these experiments owing to the large excess of *trans*-2-butene, such that the lifetime of SOZ with respect to reaction with OH is 10 min or more, much longer than the time scale of these experiments.

Pathways for Loss of Thermalized Criegee Intermediates. Clearly a second process is competing with the bimolecular aldehyde reaction to consume TCI (Figures 5 and 6). We have considered as possibilities: (1) reaction with alkene, (2) reaction with O_3, (3) loss of TCI at the reactor wall, and (4) unimolecular decomposition.

A bimolecular reaction between the TCI and the alkene was proposed in a recent study by Horie and Moortgat.[43] If the TCI reacts with the alkene, the yield of ozonide per molecule of ozone reacted should change as a function of the concentration of alkene. Figure 7 shows that the absolute yield of secondary ozonide does not change over a 12-fold increase in the alkene concentration (99−1240 ppm, see Table 4), indicating that reaction with alkene cannot explain the additional loss of TCI observed here.

Reaction between O_3 and the TCI may likewise be ruled out by the near linearity of the plot in Figure 7, indicating that the yield of secondary ozonide does not vary over a 7-fold increase in ozone concentration (1.6−11 ppm, see Table 4). The slight upward curvature in Figure 7 may be explained by the increase in cogenerated acetaldehyde with increased O_3 reacted, a change that allows the reaction with acetaldehyde to become slightly more competitive for TCI in the reaction zone. In order for

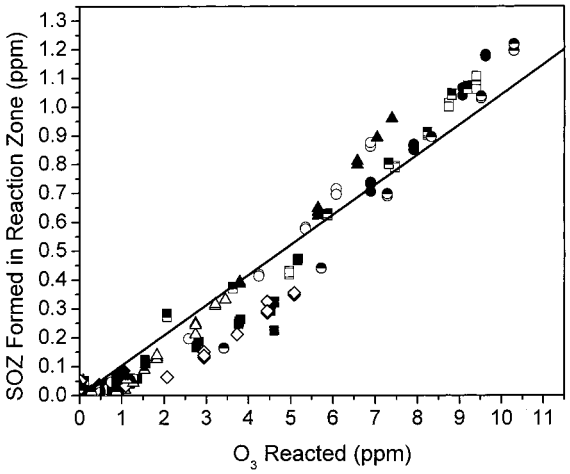

Figure 7. Flow tube data corrected for amount of SOZ formed postinjector and plotted as a function of ozone reacted. The amount of SOZ formed after the injector (region C, Figure 2) is calculated and subtracted from the total amount of SOZ observed in the FTIR using the O_3-*trans*-2-butene rate constant (see text). The line is a linear regression with the intercept set to zero.

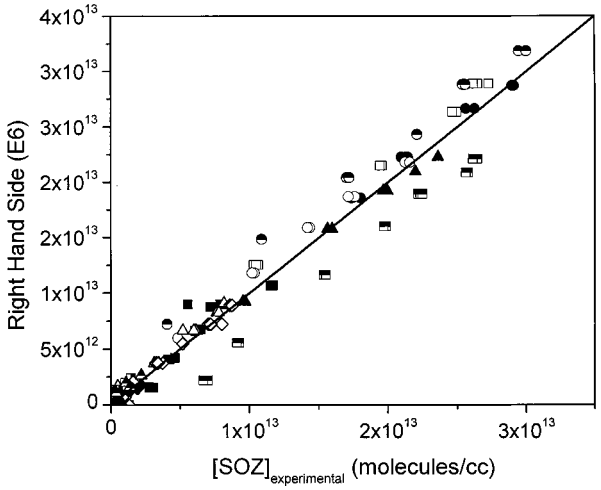

Figure 8. Experimental SOZ concentration plotted against the right-hand side of eq E6, for all flow tube experiments. The ratio k_2/k_3 has been adjusted to obtain a linear regression slope of 1 (represented by the line, see text).

another compound to be responsible for the excess disappearance of TCI, it would need to have a concentration that was independent of the *trans*-2-butene and ozone concentrations and have a lifetime of approximately 0.01 s with respect to reaction with TCI (see Figure 7). This suggests that the loss process that competes with aldehyde reaction is unimolecular.

A possible unimolecular process that could explain the rapid disappearance of TCI is wall loss. We have investigated the potential importance of wall losses by (1) comparing flow tube experiments performed in an uncoated flow tube and a tube coated with halocarbon wax, (2) estimating diffusional losses in the flow tube, (3) comparing flow tube experiments to batch reactor experiments, and (4) comparison with similar flow tubes in other research groups.

Three experiments, 10.26.99, 10.29.99a, and 10.29.99b, were performed in a flow tube coated with approximately 1 cm^3 of halocarbon wax (Halocarbon Grease Series 1500, Halocarbon Products Corp.), dissolved in approximately 200 mL of hydrofluoroether solvent (3M HFE-71DE), and allowed to dry for 2 days after which it was purged with dry nitrogen for approximately 18 h. No difference was observed between the results obtained in the coated and uncoated flow tubes (Table 4 and Figure 8), indicating that wall losses in the flow tube are insignificant.

An estimate of the first-order rate coefficient for diffusion of TCI to the walls may be obtained from

$$k_{\text{diff}} \approx \frac{4D}{x^2} \qquad \text{(E1)}$$

where D is the diffusion coefficient for the TCI and x is the average distance to the wall.[44] Using this simple calculation, k_{diff} in the flow tube is $\sim 0.2\ s^{-1}$; for the FTIR cell, it is $0.002\ s^{-1}$.

The surface area-to-volume ratio (S/V) is 2 cm^{-1} for the flow tube and 0.2 cm^{-1} for the FTIR cell. Thus, if the unimolecular disappearance of the TCI was dominated by wall losses, a significant difference in the results obtained from the flow tube and the static-cell experiments would be expected, with the ratios obtained from the batch reactor lower than those from the flow tube. The results from the static-cell experiments give a ratio $k_{\text{dec}}/k_{\text{ald}}$ of $7.5 \times 10^{13}-2.5 \times 10^{14}$, in good agreement with that obtained in the flow tube ($1.6 \times 10^{13}-1.6 \times 10^{14}$), corroborating the notion that wall losses are negligible for the measurements presented here.

Seeley et al. [45] performed extensive wall loss studies on a flow tube with dimensions nearly identical to the flow tube used for this work. Using chlorine atoms, which are known to react rapidly with untreated glass, they found that wall losses decreased as the pressure in the flow tube was increased, even under turbulent conditions, and that $k_w \ll 10\ s^{-1}$ for atmospheric pressure. They also note that for pressures near 1 atm, under turbulent flow conditions, wall losses of Cl atoms were unchanged by coating their flow tube with a halocarbon wax. Similar results were observed for CF_3O and CF_2O_2 radicals in a turbulent flow tube.[46] Wall losses in the flow tube used in this study are thus expected to be minimal.

Our evidence indicates that reaction with O_3, alkene, and wall losses do not explain the additional loss pathway for TCI formed in the *trans*-2-butene$-O_3$ reaction. The most plausible explanation is unimolecular decomposition.

Analytical Solution. The complete set of reactions that describes the chemistry in the flow tube experiments is shown in Table 2 and was used to provide a time-resolved numerical solution that allows calculation of absolute rate coefficients. The numerical solution includes detailed secondary chemistry; however, the chemistry in these experiments is essentially described by four reactions. Using the following simplified set of reactions, we can derive an analytical solution for the ratio of decomposition and reaction with aldehyde:

$$CH_3CH{=}CHCH_3 + O_3 \xrightarrow{k_{t2b-O3}} 0.18CH_3CHOO + CH_3CHO + 0.63OH \quad \text{(R6)}$$

$$CH_3CHOO + CH_3CHO \xrightarrow{k_{ald}} \text{secondary ozonide (SOZ)} \quad \text{(R7)}$$

$$CH_3CHOO \xrightarrow{k_{dec}} \text{decomposition products (P)} \quad \text{(R8)}$$

$$OH + CH_3CH{=}CHCH_3 \rightarrow\rightarrow \sim 2CH_3CHO \quad \text{(R9)}$$

Reaction R9 is a simplification of the OH−alkene chemistry in the absence of NO_x, and production of two molecules of acetaldehyde from this reaction is an overestimation.

Using this mechanism, the concentration of secondary ozonide can be determined as a function of k_{dec}/k_{ald} and the amount of ozone reacted. Since both $[O_3]_t$ and $[SOZ]_t$ are known, the parameter k_{dec}/k_{ald} can be determined by fitting the final expression E5 to the experimental data. From eqs R7 and R8, the following expression may be derived:

$$\frac{d[SOZ]}{d[P]} = \frac{k_{ald}}{k_{dec}}[CH_3CHO] \qquad (E2)$$

From the stoichiometry of eqs R6−R9, one can see that, for every O_3−alkene reaction, 0.18 mol of CH_3CHOO and 2.3 mol of CH_3CHO are formed. Provided TCI is converted either to SOZ or P, and defining ΔO_3 as $[O_3]$(initial) − $[O_3]$(time t), then at any time t

$$\Delta O_3 = \frac{[CH_3CHOO] + [P] + [SOZ]}{0.18} = \frac{[CH_3CHO]}{2.3} \qquad (E3)$$

Simplifying eq E3 by recognizing that for $t > 0$ the concentration of TCI is much smaller than the sum of the concentrations of the secondary ozonide and decomposition product concentrations ($[P] + [SOZ] \gg [CH_3CHOO]$, $[SOZ] \sim 10^{12}-10^{13}$ and $[CH_3CHOO] \sim 10^{10}$ molecules/cm^3), and substituting for $[CH_3CHO]$ in eq E2 provides the following expression

$$\frac{d[SOZ]}{d[P]} = k([P] + [SOZ]) \qquad (E4)$$

where $k = (2.3/0.18)(k_{ald}/k_{dec})$. Integrating (with t held constant) and substitution for [P] gives the expression

$$[SOZ] = \frac{\ln(0.18k\Delta[O_3] + 1)}{k} + 0.18\Delta[O_3] \qquad (E5)$$

The measured SOZ concentrations for all experiments are plotted against the right-hand side of eq E5 using the calculated O_3 concentrations in Figure 8. Varying k such that the linear regression slope is 1 gives the ratio of k_{dec} to k_{ald}. The k_{dec}/k_{ald} values calculated for each experiment are shown in Table 4 and are in good agreement with the results obtained from the complete numerical model. The average for the whole data set (Figure 8) is $(7.2 \pm 4.4) \times 10^{13}$ molecules cm^{-3}. Agreement between the numerical and analytical solutions demonstrates that the secondary reactions have a minimal effect on the chemistry.

Numerical Analysis. Numerical analysis of the flow tube experiments both provides a somewhat more accurate analysis and resolves the time-dependent dynamics of the kinetic experiments. The full set of equations describing the chemistry is shown in Table 2. The rate coefficients for the decomposition of the TCI (k_{dec}) and reaction of the TCI with aldehyde (k_{ald}) were the only adjustable parameters in the model; these were varied to obtain a best fit for each experiment. To a degree, changes in one parameter can be offset by changes in the same direction of the other parameter. For example, $k_{dec} = 70$ s^{-1} and $k_{ald} = 9 \times 10^{-13}$ cm^3 molecule^{-1} s^{-1} give a very similar model result as using $k_{dec} = 60$ s^{-1} and $k_{ald} = 8 \times 10^{-13}$ cm^3 molecule^{-1} s^{-1} (see Figure 9). However, this apparent compensation only occurs within a small range of values (less than ±15%). Figure 9 shows the model sensitivity for varying values of k_{ald} and k_{dec} while holding k_{ald}/k_{dec} constant. Comparing the model line for $k_{dec} = 70$ and $k_{ald} = 80 \times 10^{-14}$ to that for $k_{dec} = 7$ and $k_{ald} = 8 \times 10^{-14}$ (s^{-1} and cm^3 molecule^{-1} s^{-1}, respectively), it is clear that even for the same value of the ratio

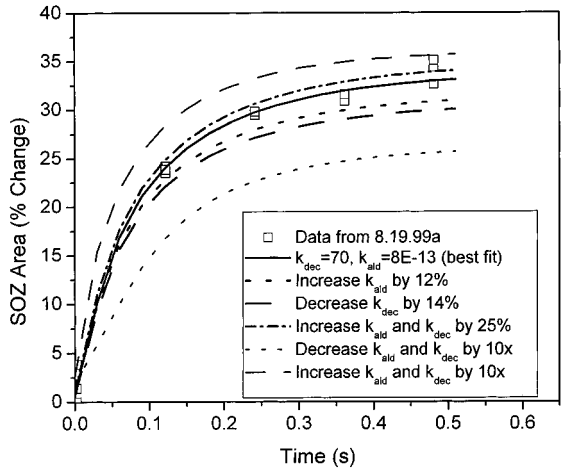

Figure 9. Sensitivity of calculated SOZ to k_{ald} and k_{dec} for experiment 8.19.99a. The solid line indicates the best fit.

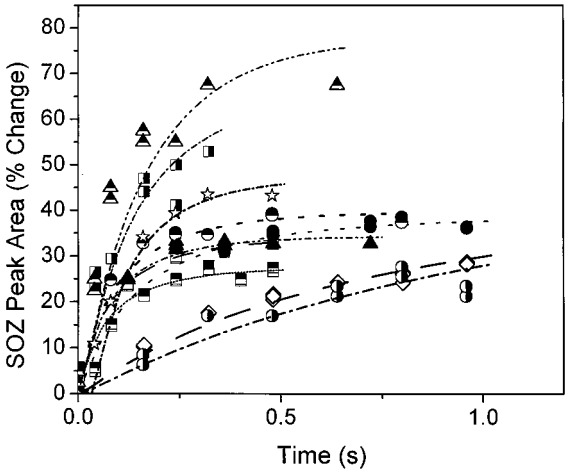

Figure 10. Selected CH_3CHOO kinetics experiments, plotted as percent change from maximum SOZ vs time (seconds). The lines represent the best-fit model curves for these experiments.

k_{ald}/k_{dec}, the results are very different, the latter pair of values resulting in a smaller initial slope and approximately 30% lower maximum SOZ concentration.

The temporal behavior of [SOZ] is determined by the concentration of TCI at time t, $[TCI]_t$. With $k_{dec} = 700$ s^{-1} and $k_{ald} = 8 \times 10^{-12}$ cm^3 molecule^{-1} s^{-1}, $[TCI]_t$ is approximately 10^{10} molecules cm^{-3}, large enough for the model output to change significantly when the rate constants are varied. As k_{ald} and k_{dec} are increased, $[TCI]_t$ approaches zero, resulting in convergence of the model output, explaining the greater sensitivity to decreasing rate coefficients in contrast to increasing them (Figure 9).

The data from 10 of the 16 kinetics experiments, including one carried out in a coated flow tube, plotted after converting injector position to reaction time and SOZ peak area to percent change in SOZ peak area, are shown in Figure 10, along with the calculated best fits. Averages are 76 s^{-1} for decomposition and 1.0×10^{-12} cm^3 molecule^{-1} s^{-1} for the bimolecular reaction with acetaldehyde (Table 4).

Figure 11a−c is included to show an intuitive picture of the competing processes in the flow tube experiments. In this figure, the abscissa shows the calculated acetaldehyde concentration rather than time. For each point (1) the quantity of CH_3CHOO formed is calculated by multiplying the extent of reaction by the CH_3CHOO yield of 0.185, (2) the amount of SOZ formed in the reaction zone is calculated by subtracting from the

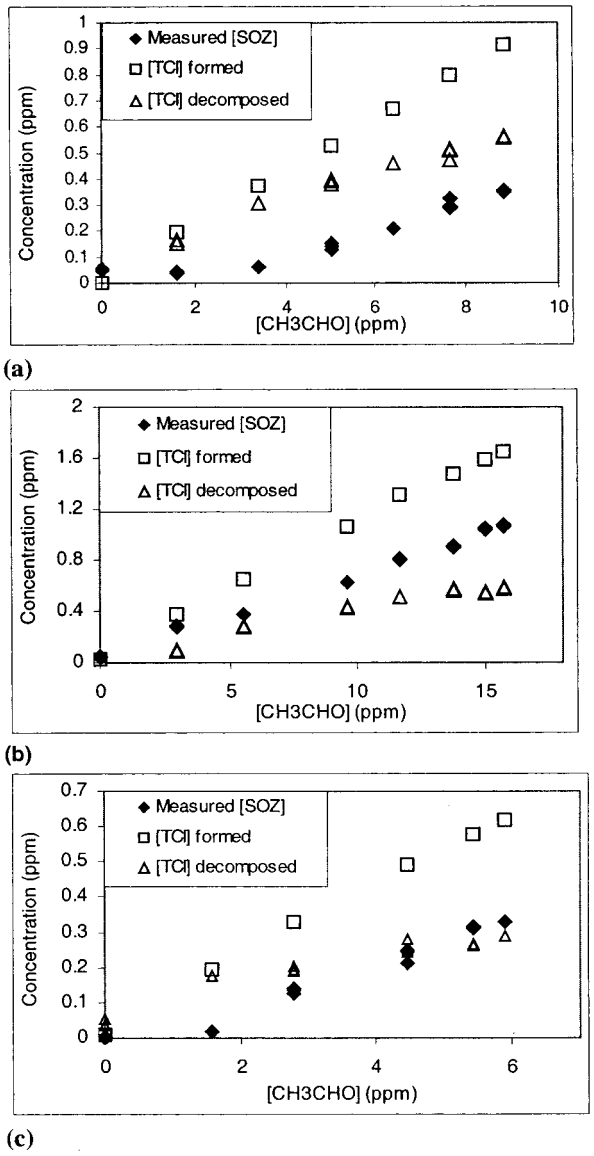

Figure 11. SOZ, total TCI, and decomposed TCI in the reaction zone. The open squares show the TCI generated, calculated from the *trans*-2-butene−O_3 reaction rate. The solid diamonds indicate measured SOZ (SOZ formed post-reaction zone has been subtracted). The open triangles show the difference between total TCI and SOZ formed in the reaction zone, which is assumed to equal decomposed TCI (see text). Initial conditions were (a) experiment 9.3.99, $[T2B]_0 = 140$ ppm, $[O_3]_0 = 11$ ppm; (b) experiment 9.1.99, $[T2B]_0 = 1200$ ppm, $[O_3]_0 = 9.8$ ppm; (c) experiment 8.30.99, $[T2B]_0 = 1190$ ppm, $[O_3]_0 = 3.7$ ppm.

measured [SOZ] the TCI present at the injector and any TCI that is formed postinjector, and (3) the difference between the first two values, assumed to equal the amount of decomposed CH_3CHOO, is calculated. Figure 11a−c shows that there are three regimes; in (a) decomposition dominates, in (b) reaction with acetaldehyde dominates, and in (c) the two processes are competitive. The data are quite scattered at low acetaldehyde concentrations because these data correspond to low SOZ concentrations, which are more difficult to measure. Inspection of Figure 11a−c shows that the "crossover" region, where reaction with acetaldehyde begins to dominate the decomposition channel, happens at acetaldehyde concentrations of approximately 5−10 ppm for all three cases, corresponding to a lifetime of TCI with respect to reaction with acetaldehyde of approximately 0.01 s, consistent with a decomposition rate coefficient of 76 s^{-1} ($\tau = 0.013$ s).

Uncertainty Analysis. The uncertainties reported in the averages in Table 4 reflect the full range of calculated values. However, additional, systematic uncertainties must be taken into consideration. The results from the model were most sensitive to the yield of TCI. The range of measured values (see above) is 0.185 ± 0.06. Increasing the TCI yield from the reaction of ozone with *trans*-2-butene by 30% increased the steady-state concentration of TCI by a factor of 2, resulting in a negligible change in the calculated decomposition rate, and decreased the calculated rate coefficient for reaction with acetaldehyde by a factor of 4.5. Decreasing the TCI yield by 30% decreased the steady-state concentration of TCI by a factor of 3, resulting in a decrease in the decomposition rate coefficient by a factor of 2.7 and an increase in the aldehyde rate coefficient by a factor of 5.5. Decreasing the yield of TCI has more impact on the rate coefficient because it decreases the already low steady-state concentration of TCI. The other parameters in the model that have potential to affect the results of this analysis are the rate coefficient of ozone reaction with *trans*-2-butene, which affects the rate of generation of TCI and aldehydes, the rate coefficient of OH radical with *trans*-2-butene, which affects the generation rate of the RO_2 radicals that are eventually converted to acetaldehyde, the self-reaction rate coefficient of the RO_2 radicals, because this self-reaction generates acetaldehyde, and the yield of acetaldehyde from the reaction of ozone with *trans*-2-butene. Changing the rate coefficient of ozone reaction with *trans*-2-butene by 35% (the recommended uncertainty[47]) changed both the decomposition rate and reaction rate with acetaldehyde by 30% in the opposite direction (increasing k_{t2b-O3} decreased both k_{ald} and k_{dec}). Changing the rate coefficient of the reaction of OH with *trans*-2-butene by ±20% (the recommended uncertainty[48]) had a negligible effect on the results obtained for these experiments. Varying the rate coefficient for the self-reaction of the RO_2 radicals resulting from the OH reaction with *trans*-2-butene by a factor of 5 in either direction (this is likely a reasonable estimate of the uncertainty because the rate coefficients were approximated by analogy to similar RO_2 radicals) had no effect on the decomposition rate obtained from this analysis and only changed the acetaldehyde rate coefficient by 20% in the opposite direction (increasing k_{OH-t2b} decreased k_{ald}). Changing the yield of acetaldehyde from the reaction of ozone with *trans*-2-butene by 20% (the recommended uncertainty was ±8−12%[49]) also had no effect on the decomposition rate coefficient but changed the acetaldehyde rate coefficient by 15% in the opposite direction. Combining these sources of uncertainty with the random experimental error results in an overall uncertainty of a factor of 3 for the decomposition rate and a factor of 6 for the bimolecular rate coefficient for acetaldehyde reacting with CH_3CHOO.

Discussion

Some previous studies have addressed decomposition of thermalized Criegee intermediates. In general, it is expected that the decomposition rate will increase with increasing substitution to the TCI (i.e., from CH_2OO to CH_3CHOO to $(CH_3)_2COO$). The reason for this trend is the availability of the isomerization channel to the vinyl hydroperoxide (R1c), which cannot occur for CH_2OO, can occur for *syn*- but not *anti*-CH_3CHOO, and which can occur for all $(CH_3)_2COO$. This unimolecular process appears to have a low activation energy,[39] which enhances the rate of decomposition of the TCI. Thus as the availability of this channel increases with increasing substitution to the TCI, so the unimolecular rate coefficient increases. Olzmann et al.[39] estimated 0.3 and 250 s^{-1} as the rate coefficients for the

decomposition of CH_2OO and $(CH_3)_2COO$, respectively. Herron et al. [31] used relative rate arguments to estimate that for CH_3CHOO, $4 \times 10^{-3}\ s^{-1} < k_{dec} < 20\ s^{-1}$. Horie and Moortgat[13] probed consumption of formaldehyde and formation of products to derive rate coefficients of formaldehyde with CH_2OO and CH_3CHOO in a CSTR reactor. The residence time in the CSTR was not varied, but the formaldehyde concentration was, in direct analogy to our batch reactor experiments. Using a model, they derived rate coefficients of 2×10^{-17} and 4×10^{-16} for the formaldehyde reaction with CH_2OO and CH_3CHOO, respectively, and inferred a decomposition channel for the CH_3CHOO (but not CH_2OO) with a rate coefficient of $2.5\ s^{-1}$. Although these experimental values are estimates with large uncertainties, they are in reasonable agreement with our value for the decomposition rate ($76\ s^{-1}$). Although our measurement for the unimolecular decomposition rate coefficient for CH_3CHOO fits nicely between Olzmann et al.'s calculated values for CH_2OO and $(CH_3)_2COO$, no conclusions can be drawn from this. The most accurate theoretical calculations for activation energies have uncertainties of more than 4 kcal mol^{-1}, which result in uncertainties in the unimolecular rate coefficient of almost 3 orders of magnitude at room temperature.

No measurements have been reported for the reaction of CH_3CHOO with acetaldehyde. Our value, 1.1×10^{-12} cm^3 $molecule^{-1}\ s^{-1}$, is at the upper end of the wide range of previous estimates for the reaction of HCHO and CH_3CHO with CH_2OO (Table 1).

Atmospheric Implications. Reaction of TCI with water in the atmosphere is of particular interest because the proposed products are peroxides and organic acids. Hydroperoxides have been implicated in the forest decline observed in Europe and North America,[50] and organic acids have been identified as a major source of free acidity in rain in rural areas as well as a contributor to secondary organic aerosol formation (e.g., ref 19). Owing to the high concentration of water in the atmosphere, this reaction may be the dominant atmospheric sink for TCI, and, if it is, may be a significant source of peroxides and organic acids in the atmosphere.

Inspection of the TCI rate coefficients and reactant partner concentrations (Table 1) reveals that reactions with SO_2 and H_2O have potential to be important in the troposphere. If we assume that the relative rates for CH_3CHOO with acetaldehyde and SO_2 are the same as those suggested by Atkinson and Lloyd[30] for CH_2OO with formaldehyde and SO_2 ($k_{SO_2}/k_{HCHO} \sim 4$[8]), we can obtain new estimates for the rate coefficient for reaction of CH_3CHOO with SO_2 of $\sim 4 \times 10^{-12}$ and with water of $\sim 2 \times 10^{-16}$ cm^3 $molecule^{-1}\ s^{-1}$ based on ($k_{H_2O}/k_{SO_2} \sim 5 \times 10^{-5}$ [51]). For an ambient SO_2 concentration of 20 ppb (see Table 1), this corresponds to a loss of TCI of $2\ s^{-1}$ with respect to reaction with SO_2. For a relative humidity of 60% (14 000 ppm of H_2O at 298 K), the loss of TCI with respect to reaction with water is approximately $60\ s^{-1}$; 100% relative humidity would give $\sim 120\ s^{-1}$. Thus, from the results presented here, it appears that decomposition of TCI could occur much faster than reaction with SO_2 and on the same time scale as the bimolecular reaction with water, and may be another important loss process for thermalized Criegee intermediates in the troposphere, reducing production of acids and hydroperoxides from these reactions in the atmosphere.

References and Notes

(1) Guenther, A.; Hewitt, C. N.; Erickson, D.; Fall, R.; Geron, C.; Graedel, T.; Harley, P.; Klinger, L.; Lerdau, M.; McKay, W. A.; Pierce, T.; Scholes, B.; Steinbrecher, R.; Tallamraju, R.; Taylor, J.; Zimmerman, P. *J. Geophys. Res.* **1995**, *100* (D5), 8873−92.

(2) N. R. C. *Rethinking the Ozone Problem in Urban and Regional Air Pollution*; Seinfeld, J. H., Ed.; National Research Council, National Academy Press, 1991.

(3) Cremer, D.; Gauss, J.; Kraka, E.; Stanton, J. F.; Bartlett, R. J. *Chem. Phys. Lett.* **1993**, *209* (5, 6), 547−556.

(4) Gutbrod, R.; Kraka, E.; Schindler, R. N.; Cremer, D. *J. Am. Chem. Soc.* **1997**, *119*, 7330−42.

(5) Anglada, J. M.; J. Bofill, M.; Olivella, S.; Sole, A. *J. Am. Chem. Soc.* **1996**, *118*, 4636−47.

(6) Anglada, J. M.; Crehuet, R.; Bofill, J. M. *Chem. Eur. J.* **1999**, *5*, 1809.

(7) Hatakeyama, S.; Akimoto, H. *Res. Chem. Intermed.* **1994**, *20* (3/4/5), 503−24.

(8) Su, F.; Calvert, J. G.; Shaw, J. H. *J. Phys. Chem.* **1980**, *84*, 239−46.

(9) Niki, H.; Maker, P. D.; Savage, C. M.; Breitenbach, L. P. *J. Phys. Chem.* **1981**, *85*, 1024.

(10) Kan, C. S.; Su, F.; Calvert, J. G.; Shaw, J. H. *J. Phys. Chem.* **1981**, *85*, 2359.

(11) Hatakeyama, S.; Kobayashi, H.; Akimoto, H. *J. Phys. Chem.* **1984**, *88*, 4736−9.

(12) Hatakeyama, S., Kobayashi, H.; Lin, Z.-Y.; Takagi, H.; Akimoto, H. *J. Phys. Chem.* **1986**, *90*, 4131−5.

(13) Horie, O.; Moortgat, G. K. *Atmos. Environ.* **1991**, *25A* (9), 1881−1896.

(14) Niki, H., Maker, P. D.; Savage, C. M.; Breitenbach, L. P. *Chem. Phys. Lett.* **1977**, *46*, 327.

(15) Horie, O.; Neeb, P.; Moortgat, G. K. *Int. J. Chem. Kinet.* **1997**, *29* (6), 461−468.

(16) Paulson, S. E.; Seinfeld, J. H. *Environ. Sci. Technol.* **1992**, *26*, 1165−1173.

(17) Keen, W. C.; Galloway, J. N. *J. Geophys. Res.* **1986**, *91*, 14466.

(18) Criegee, R. *Angew. Chem., Intt. Ed. Eng.* **1975**, *14* (11), 745−752.

(19) Finlayson-Pitts, B. J.; Pitts, J. *Atmospheric Chemistry*: *Fundamentals and Experimental Techniques*; Wiley: New York, 1986.

(20) Fenske, J. D.; Kuwata, K. T.; Houk, K. N.; Paulson, S. E., in progress.

(21) Atkinson, R. *J. Phys. Chem. Ref. Data* **1997**, *26* (2), 215−90.

(22) Niki, H. Maker, P. D.; Savage, C. M.; Breitenback, L. P.; Hurley, M. D. *J. Am. Chem. Soc.* **1987**, *91*, 941−6.

(23) Gutbrod, R.; Schindler, R. N.; Kraka, E.; Cremer, D. *Chem. Phys. Lett.* **1996**, *252*, 221−229.

(24) Horie, O.; Schafer, C.; Moortgat, G. K. *Int. J. Chem. Kinet.* **1999**, *31*, 261−9.

(25) Rickard, A. R.; Johnson, D.; McGill, C. D.; Marston, G. *J. Phys. Chem. A* **1999**, *103* (38), 7656−64.

(26) Hasson, A. S.; Paulson, S. E.

(27) Neeb, P.; Horie, O.; Moortgat, G. K. *Tetrahedron Lett.* **1996**, *37* (52), 9297−300.

(28) Becker, K. H.; Bechara, J.; Brockmann, K. J. *Atmos. Environ.* **1993**, *27A*(1), 57−61.

(29) Niki, H.; Maker, P. D.; Savage, C. M.; Breitenback, L. P. *Environ. Sci. Technol.* **1983**, *17*, 312a−322a.

(30) Atkinson, R.; Lloyd, A. C. *J. Phys. Chem. Ref. Data* **1984**, *13* (2), 315−444.

(31) Herron, J. T.; Martinez, R. I.; Huie, R. E. *Int. J. Chem. Kinet.* **1982**, *14*, 201−24.

(32) Fajgar, R.; Vitek, J.; Haas, Y.; Pola, J. *Tetrahedron Lett.* **1996**, *37* (19), 3391−4.

(33) Fajgar, R.; Vitek, J.; Haas, Y.; Pola, J. *J. Chem. Soc., Perkin Trans. 2* **1999**, 239−48.

(34) Neeb, P.; Horie, O.; Moortgat, G. K. *Chem. Phys. Lett.* **1995**, *246*, 150−6.

(35) Thamm, J.; Wolff, S.; Turner, W. V.; Gab, S.; Thomas, W.; Zabel, F.; Fink, E. H.; Becker, K. H. *Chem. Phys. Lett.* **1996**, *258*, 155−8.

(36) Kuhne, H.; Vaccani, S.; Ha, T.-K.; Bauder, A.; Gunthard, H. H. *Chem. Phys. Lett.* **1976**, *38*, 449.

(37) Cremer, D.; Kraka, E.; M. McKee, L.; Radhakrishnan, T. P. *Chem. Phys. Lett.* **1991**, *187* (5), 491−493.

(38) Ponec, R.; Yuzhakov, G. *J. Org. Chem.* **1997**, *62*, 2757−2762.

(39) Olzmann, M.; Kraka, E.; Cremer, D.; Gutbrod, R.; Anderson, S. *J. Phys. Chem. A* **1997**, *101*, 9421−29.

(40) Horie, O.; Neeb, P.; Limbach, S.; Moortgat, G. K. *Geophys. Res. Lett.* **1994**, *21* (14), 1523−1526.

(41) Simonaitis, R.; Olszyna, K. J.; Meagher, J. F. *Geophys. Res. Lett.* **1991**, *18* (1), 9−12.

(42) Neeb, P.; Horie, O.; Moortgat, G. K. *Int. J. Chem. Kinet.* **1996**, *28*, 721−30.

(43) Horie, O.; Moortgat, G. K. *Acc. Chem. Res.* **1998**, *31*, 387−96.

(44) Seinfeld, J. H. *Atmospheric Chemistry Physics of Air Pollution*; John Wiley and Sons: New York, 1986.

(45) Seeley, J. V.; Jayne, J. T.; Molina, M. J. *Int. J. Chem. Kinet.* **1993**, *25*, 571−94.

(46) Bourbon, C.; Brioukov, M.; Hanoune, B.; Sawerysyn, J. P.; Devolder, P. *Chem. Phys. Lett.* **1996**, *254*, 203−12.
(47) Atkinson, R. *J. Phys. Chem. Ref. Data* **1992**, 1−216.
(48) Atkinson, R. *Chem. Rev.* **1985**, *85*, 69−201.
(49) Tuazon, E. C.; Aschmann, S. M.; Arey, J.; Atkinson, R. *Environ. Sci. Technol.* **1997**, *31*, 3004−9.
(50) Hewitt, N.; Terry, G. *Environ. Sci. Technol.* **1992**, *26*, 1890.
(51) Cox, R. A.; Penkett, S. A. *J. Chem. Soc., Faraday Trans. 1* **1972**, *68*, 1735.
(52) Gab, S.; Hellpointer, E.; Turner, W. V.; Korte, F. *Lett. Nature* **1985**, *316*, 535−6.
(53) Hewitt, C. N.; Kok, G. L. *J. Atmos. Chem.* **1991**, *12*, 181−94.
(54) Calvert, J. G.; Stockwell, W. R. *Environ. Sci. Technol.* **1983**, *17*, 428A.